

# Asymmetric Chiral Metamaterial Multi-Band Circular Polarizer Based on Combined Twisted Double-Gap Split-Ring Resonators

Wenshan Yuan<sup>1</sup>, Honglei Zhang<sup>2</sup>, and Yongzhi Cheng<sup>3, \*</sup>

**Abstract**—In this paper, an ultrathin asymmetric chiral metamaterial multi-band circular polarizer using combined twisted double-gap split-ring resonators (DGSRs) is proposed and investigated. Experiment and numerical simulations are in good agreement, indicating that when a  $y$ -polarized wave is incident on this chiral metamaterial propagating along  $-z$  direction, the right circularly polarized (RCP) wave is emitted at 5.58 GHz and 9.34 GHz, while left circularly polarized (LCP) wave is excited at 6.41 GHz and 7.65 GHz, in addition to large polarization extinction ratio of more than 18 dB at the four resonant frequencies. The surface current distributions are studied to illustrate the transformation behavior for both circular polarizations.

## 1. INTRODUCTION

Metamaterials (MMs), a rapidly developing cutting-edge research field in the last decade, possess exotic properties and capability for the manipulations of the behaviors of the incident electromagnetic (EM) or light wave radiation which are not found in nature [1–3]. Since Pendry theoretically predicted that a chiral route can be used to achieve negative refraction [4–6], chiral metamaterials (CMMs) as a class of MMs have attracted more and more interest. From microwave to optical frequency range exotic EM properties and a wider set of functionalities have been achieved by special CMMs design such as giant gyrotropy [7], optical activity [8–10], circular dichroism (CD) effect [11–13] asymmetric transmission (AT) effect [14–17]. Essentially, CMMs can function as those unusual EM properties which mainly arise from cross-coupling of chiral structures between the electric and magnetic fields, since they are lack of any mirror symmetry and violate neither reciprocity nor time-reversal symmetry [18].

On these peculiarities, CMMs could be used to manipulate polarization states of EM waves for achieving polarization conversion, such as linear to linear [14–17], linear to circular [19–25], and circular to circular [26]. Especially, circular polarization is an important property of EM or optical wave which has many potential applications, such as antennas [27], liquid crystal displays, and remote sensors [28, 29]. Thus, circular polarizer is an important device, which can transform incident arbitrary polarization waves into circularly polarized waves. Several efforts have been made to design various high performance circular polarizers using the MMs due to their advantages, such as high polarization conversion efficiency, and operation frequency can be scaled to different EM spectrums by the changes of geometrical parameters. For the CMMs circular polarizers, at the beginning the three-dimensional (3D) gold helical MMs have been employed to obtain broadband circular polarization with giant CD effect [12]. However, only one kind of circularly polarized waves can be transformed by such a helix CMM, which is hard to fabricate and integrate into present systems. Then, asymmetric CMMs using four double-layered U-shaped SRRs with different sizes were proposed [19], which can transform incident linearly polarized

---

*Received 21 March 2014, Accepted 17 April 2014, Scheduled 23 April 2014*

\* Corresponding author: Yongzhi Cheng (cyz0715@126.com).

<sup>1</sup> School of Information and Electrical Engineering, Hebei University of Engineering, Handan 056038, China. <sup>2</sup> School of Economics and Management, Hebei University of Engineering Handan 056038, China. <sup>3</sup> School of Optical and Electronic Information, Huazhong University of Science and Technology, Wuhan 430074, China.

waves into circularly polarized waves with different handednesses at two distinct resonances. Since then, planar spiral structure [20–22], Hilbert-shaped structure [23] and twisted split ring resonators (SRRs) with double or more concentric rings [24, 25] have been reported. However, linear to circular polarization transformation coefficients of the above structures are low. Meanwhile, weak EM energy is emitted at the transformation frequencies. In addition, there is little literature about the realization of multi-band circular polarizer [21, 22].

In this paper, an ultra-thin asymmetric CMM multi-band circular polarizer is presented, based on double-layered twisted double-gap split-ring resonators (DGSRRs) structures arranged at a  $90^\circ$  twisted angle. The two planar twisted SRRs structure with different sizes in each layer is adopted to achieve more resonant frequencies. Both experiment and simulation results indicate that circular polarization waves at different rotation directions are obtained at four distinct resonances when a  $y$ -polarized wave is incident on the CMMs propagating along  $-z$  direction. The experiment results are in good agreement with the numerical simulations.

## 2. STRUCTURE DESIGN, SIMULATION AND EXPERIMENT

The influences of the structural parameters on the linear to circular transformation properties of the bi-layer twisted DGSRRs structure have been studied systematically [25]. It is found that the functional frequency region of this asymmetric CMM can be adjusted easily by changing the dielectric layer thickness and line width of SRRs structure. The giant CD effect with high polarization extinction ratio can also be obtained by selecting these structure parameters appropriately. To achieve multi-band resonances, we can combine two different sized SRRs structures in a unit cell. As shown in Figure 1(a), the metallic DGSRRs structures with different sizes in each layer are the same; however, when fixing the first layer structure, the structure in the second layer is rotated clockwise with  $90^\circ$  along the propagating direction of EM wave.

Finally, the mirror symmetry of the whole structure is broken in the  $z$  direction and in the  $x$ - $y$  plane, due to the two-layer chiral structure copper patterns separated by the middle dielectric spacer [17]. The optimal geometry dimension parameters are as follow, in millimeters:  $p = 20$ ,  $t = 1.5$ ,  $a_1 = 8$ ,  $w_1 = 1$ ,  $g_1 = 1.5$ ,  $a_2 = 6.4$ ,  $w_2 = 0.8$ ,  $g_2 = 1.2$ . The metallic layers in both sides were modeled as a 0.017 mm copper film with an electric conductivity  $\sigma = 5.8 \times 10^7$  S/m. The FR-4 (lossy) substrate with a permittivity of 4.3 and loss tangent of 0.025 is selected as the dielectric spacer. Computer numerical simulations are performed based on the standard finite difference time domain (FDTD) method. In simulation process, the periodic boundary conditions are applied to the  $x$  and  $y$  directions and the absorbing boundary conditions to the  $z$  direction as well.

According to the optimal structure parameters, the designed model is fabricated into a  $10 \times 10$  unit cell sample ( $200 \text{ mm} \times 200 \text{ mm} \times 1.534 \text{ mm}$ ) by conventional printed circuit board (PCB) process with  $17 \mu\text{m}$ -thick copper patterns on both sides of a FR-4 (lossy) substrate, and a photograph of a portion

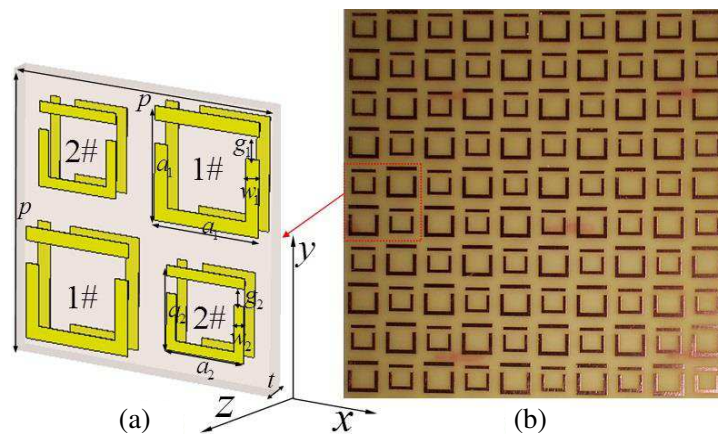


**Figure 1.** (a) Unit cell of bi-layer twisted structure, (b) the fabricated sample.

of a fabricated asymmetric CMMs sample is shown in Figure 1(b). The complex linear transmission coefficients of experimental measurements are carried out in an EM anechoic chamber [25]. Agilent PNA-X N5244A vector network analyzer connected to the two standard gain broadband linearly polarized horn antennae that produce microwaves in the range of 5–10 GHz are used to measure the MM sample. All components of the EM wave transmission for different polarizations have been measured by changing the orientation of the two horn antennas.

For both simulation and experiment, the transmission of co-polarization  $t_{yy}$  and cross-polarization  $t_{xy}$  can be obtained when the electric field of incident EM wave is along  $+y$  direction propagating along  $-z$  direction, where the first subscript denotes the polarization of the transmitted field, and the second subscript presents the polarization of the incident field. Then the linear to circular transformation transmission coefficients can be calculated by the formula of  $t_{\pm y} = \frac{1}{\sqrt{2}}(t_{xy} \pm it_{yy})$  from the simulation and experiment, where the subscript “+” denotes the RCP wave and subscript “-” the LCP wave [24, 25]. Thus, we can use this equation to describe the capability of transforming an EM wave with linear polarization to a circular polarization wave. Moreover, the substantially large or small difference (polarization extinction ration, PER) between the emitted RCP and LCP waves is calculated by  $20 \log_{10} (|t_{+x(y)}|/|t_{-x(y)}|)$ , which can be used to measure the ability for linear to circular polarization conversion. The CD effect and optical activity for the normal incident linearly polarized waves can be clearly demonstrated through the analysis of ellipticity angle  $\eta$  and polarization azimuth rotation angle  $\theta$ , which can be calculated by the following formulas:  $\eta = \arctan \left( \frac{|t_+| - |t_-|}{|t_+| + |t_-|} \right)$  and  $\theta = \frac{1}{2} (\arg(t_+) - \arg(t_-))$ , respectively [18, 20, 24], where  $t_+$  and  $t_-$  are the transmission coefficients of RCP and LCP waves.

### 3. RESULTS AND DISCUSSION

In this particular design, the good performances for the circular polarizer are only valid for the incident  $(x)y$  polarization wave propagating along  $+z$  ( $-z$ ) direction. Thus, we only give the simulated and measured co- and cross-polarization transmission coefficients ( $t_{yy}$  and  $t_{xy}$ ) for the normal incident  $y$ -polarized wave propagating in backward ( $-z$ ) directions, as shown in Figure 2. The experimental results are in good agreement with the simulations across the whole frequency range. From Figure 2, simulated (experimental) four resonant peaks (dips) are obviously observed around  $f_1 = 5.58$  (5.51) GHz,  $f_2 = 6.41$  (6.42) GHz,  $f_3 = 7.65$  (7.54) GHz and  $f_4 = 9.34$  (9.43) GHz of the linear polarization transmission coefficients  $t_{yy}$  and  $t_{xy}$  from simulation and measurement. There are slight frequency shift between simulation and measurement curves, which is mainly due to the inherent tolerances and random errors caused in fabrications and measurements. In order to demonstrate the linear to circular polarization conversion characteristics of the designed structure for incident wave, the ratio  $p_y = |t_{xy}|/|t_{yy}|$  and phase difference  $\varphi_y = \arg(t_{xy}) - \arg(t_{yy})$  are calculated from the simulated and experimental transmission coefficients  $t_{yy}$  and  $t_{xy}$ , and the corresponding results are presented in Figures 3(a) and (b). It can be observed that the values of ratio  $p_y$  are near unity, and the phase differences  $\varphi_y$  are  $91.6^\circ$  ( $92.7^\circ$ ),  $-89.1^\circ$  ( $88.7^\circ$ ),  $-91.5^\circ$  ( $-89.2^\circ$ ) and  $87.1^\circ$  ( $89.2^\circ$ ) at above four resonant frequencies, respectively. We

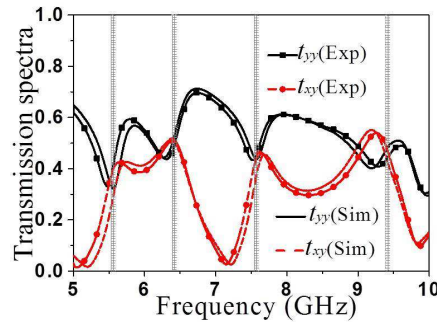


**Figure 2.** Simulated and measured linear transmission coefficients for the backward propagating in  $y$  polarization.

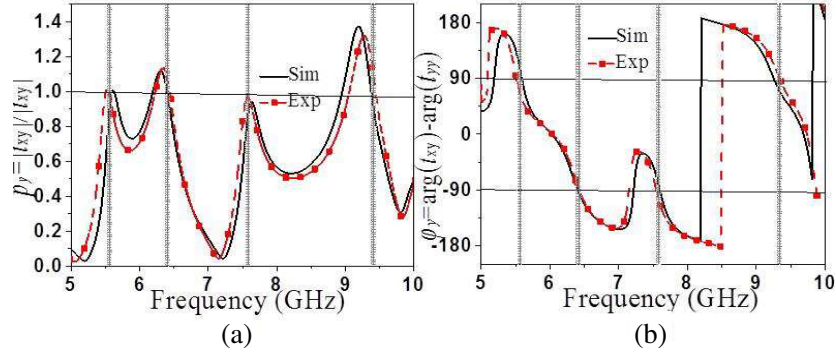


**Figure 3.** Simulated and measured (a) magnitude and (b) phase difference of linear transmission coefficients  $t_{yy}$  and  $t_{xy}$ .

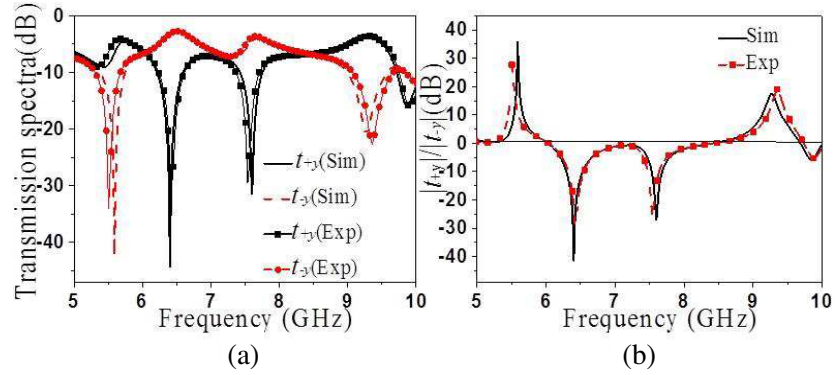
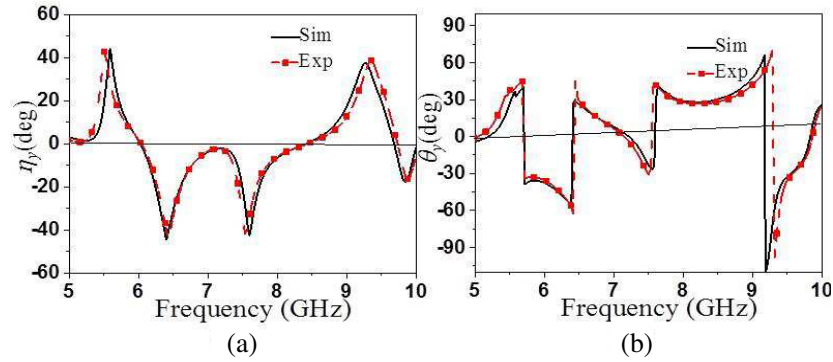


**Figure 4.** Simulated and measured (a) linear to circular transmission coefficients, (b) polarization extinction ratio (PER).

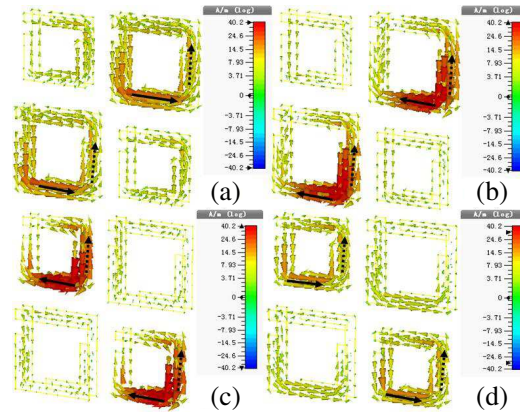
can conjecture that the resonances in Figures 3(a) and (b) corresponding to the EM coupling between the front and back layers are very strong [25], which will directly cause that nearly pure circular polarization waves are produced.

Figure 4(a) shows the simulation and experiment linear-circular transmission coefficients ( $t_{+y}$  and  $t_{-y}$ ) of the designed CMMs for the incident  $y$ -polarized wave propagating along backward ( $-z$ ) direction. From Figure 4(a), numerical (experimental) results indicate that the peak values of the RCP waves are  $-6.1$  dB ( $-5.6$  dB),  $-44.4$  dB ( $-31.4$  dB),  $-31.5$  dB ( $-31.3$  dB) and  $-3.4$  dB ( $-3.2$  dB) at 5.58 (5.51) GHz, 6.42 (6.41) GHz, 7.65 (7.54) GHz and 9.34 (9.43) GHz, respectively. While the peak values of the LCP waves are  $-42.3$  dB ( $-34$  dB),  $-2.7$  dB ( $-2.7$  dB),  $-3.7$  dB ( $-3.7$  dB) and  $-22.7$  dB ( $-21.2$  dB) at the same resonant frequencies, respectively. Furthermore, as shown in Figure 4(b), it can be clearly seen that the peak values of the polarization extinction ratios (PER) are up to 35.7 dB (27.7 dB),  $-41.5$  dB ( $-29.3$  dB),  $-26.8$  dB ( $-25.2$  dB) and 18.1 dB (2.2 dB) at the same resonant frequencies, respectively. These results further confirm that nearly pure circularly polarized waves with different handednesses are realized at above four frequencies, e.g., the transmitted waves are RCP at 5.58 (5.51) GHz and 9.34 (9.43) GHz, and the transmitted LCP waves are emitted at 6.42 (6.41) GHz and 7.65 (7.54) GHz. It means that the incident  $y$ -polarized ( $x$ -polarized) along the  $-z$  ( $+z$ ) directions wave can be converted well to the transmitted nearly pure RCP and LCP wave at the resonances after passing through the CMMs slab.

To further demonstrate the performance of the designed CMMs, Figures 5(a) and (b) show the calculated ellipticity angle  $\eta$  and polarization rotation angle  $\theta$  from the simulated and experimental transmission coefficients of RCP and LCP waves in the case of  $y$ -polarization incidence. From Figure 5(a), it can be observed that the calculated (measured) values of  $\eta_y$  are  $44.1^\circ$  ( $42.6^\circ$ ) at 5.58



**Figure 5.** Simulated and measured (a) ellipticity ( $\eta$ ) and (b) polarization azimuth rotation angle ( $\theta$ ) for the backward ( $-z$ ) propagating in  $y$  polarization.



**Figure 6.** (a) The simulated surface currents distributions of the unit cell in the case of  $y$ -polarized incident wave propagating along  $-z$  direction: RCP wave at (a)  $f_1 = 5.58$  GHz and (d)  $f_4 = 9.34$  GHz, LCP wave at (b)  $f_2 = 6.41$  GHz and (c)  $f_3 = 7.65$  GHz. The solid (dashed) line arrows represent the front (back) surface current direction.

(5.51) GHz,  $-44.5^\circ$  ( $43.7^\circ$ ) at 6.42 (6.41) GHz,  $-42.6^\circ$  ( $41.7^\circ$ ) at 7.65 (7.54) GHz and  $37.4^\circ$  ( $38.7^\circ$ ) at 9.34 (9.43) GHz, respectively for the  $y$ -polarized incident wave. It means that the emitted fields are close to pure circular polarization at above four resonant frequencies. Furthermore, it can also be found that the ellipticity  $\eta_y$  equals zero at 6.03 GHz and 8.43 GHz, where the transmitted waves are linearly polarized but rotating a certain angle. As shown in Figure 5(b), the values of calculated (measured) polarization azimuth rotation angles  $\theta_y$  are changed to  $-38.6^\circ$  ( $-36.2^\circ$ ) and  $29.3^\circ$  ( $27.7^\circ$ ) with respect to the incident linearly  $y$ -polarized wave when  $\eta_y = 0^\circ$ , revealing huge optical activity.

From previous researches, it can be learned that the giant CD effect for high performance circular polarizer intrinsically originates from the interlayer near-field coupling between two twisted layers [13, 25, 30, 31]. In detail, the RCP wave radiation arises from fundamental electric resonance mode (similarly to the electric dipole resonance mode), and the LCP wave is caused by fundamental magnetic resonance mode (similarly to coupled magnetic dipoles resonance mode) [25]. To better understand the mechanism of resonances, the surface current distributions on the upper and bottom layers for normal incident  $y$ -polarized wave propagating along  $-z$  direction have been examined, as shown in Figure 6. Obviously, the first couple resonances ( $f_1 = 5.58$  GHz and  $f_2 = 6.41$  GHz) are mainly caused by the larger structure, while the second couple resonances ( $f_3 = 7.65$  GHz and  $f_4 = 9.34$  GHz) are mainly attributed to the smaller one. Taking a step further, from Figures 6(a) and (d), at the first and fourth resonances ( $f_1$  and  $f_4$ ), the directions of the surface currents of the two layers structure for both larger and smaller structures are the same, i.e., clockwise, as denoted by black arrows which are symmetric

current resonance modes and indicating stronger electrical resonances, leading to RCP wave emitting. While at second and third resonances ( $f_2$  and  $f_3$ ), the directions of the surface currents of the top and bottom layer structures are opposite, which are asymmetric resonance modes and indicating stronger magnetic resonances, finally leading to LCP waves. The surface current distributions features are similar to the previous single SRRs structure in previous study [25], which has similar current distributions in the symmetric and asymmetric resonance modes [30]. These features of coupling resonances between metallic layers can further validate that our proposed asymmetric CMM structure can function as an ultrathin (the thickness of the MM is smaller than  $\lambda/20$  with  $\lambda$  the operating wavelength) multi-band circular polarizer.

#### 4. CONCLUSION

In conclusion, a combined asymmetric chiral bi-layered structure based on twisted DGSRRs is proposed. Both simulation and experiment demonstrate that it can convert a linearly polarized wave to an RCP wave at 5.58 (5.51) GHz and 9.34 (9.43) GHz, and LCP waves at 6.42 (6.41) GHz and 7.65 (7.54) GHz, respectively. The measured results are in good agreement with the numerical simulations, indicating a large polarization extinction ratio of more than 18 dB at the four frequencies. The surface current distributions are studied to understand that the larger twisted SRRs play a great role in the CMM at the lower frequency while the one with smaller size is responsible for higher resonances. In addition, this asymmetric CMM is easy to be scaled into terahertz and even optical frequencies due to the geometry scalability. Furthermore, the proposed asymmetric CMMs can give a more profound understanding on chirality and to offer flexibility in the investigation of novel EM wave manipulation device.

#### REFERENCES

1. Veselago, V. G., "The electrodynamics of substances with simultaneously negative values of  $\epsilon$  and  $\mu$ ," *Sov. Phys. Uspekhi*, Vol. 10, 509, 1968.
2. Shelby, R. A., D. R. Smith, and S. Schultz, "Experimental verification of a negative index of refraction," *Science*, Vol. 292, 77–79, 2001.
3. Cai, W. and V. Shalaev, *Optical Metamaterials: Fundamentals and Applications*, Springer Science + Business Media, LLC, 2010.
4. Pendry, J. B., "A chiral route to negative refraction," *Science*, Vol. 306, No. 19, 1353–1355, 2004.
5. Plum, E., J. Zhou, J. Dong, V. A. Fedotov, T. Koschny, C. M. Soukoulis, and N. I. Zheludev, "Metamaterial with negative index due to chirality," *Phys. Rev. B*, Vol. 79, 035407-6, 2009.
6. Wang, B., T. Koschny, M. Kafesaki, and C. M. Soukoulis, "Chiral metamaterials: Simulations and experiments," *J. Opt. A: Pure Appl. Opt.*, Vol. 11, 114003-10, 2009.
7. Rogacheva, A. V., V. A. Fedotov, A. S. Schwanecke, and N. I. Zheludev, "Asymmetric propagation of electromagnetic waves through a planar chiral structure," *Phys. Rev. Lett.*, Vol. 97, No. 17, 177401-4, 2006.
8. Singh, R., E. Plum, W. L. Zhang, and N. I. Zheludev, "Highly tunable optical activity in planar achiral terahertz metamaterials," *Opt. Express*, Vol. 18, 13425–13430, 2010.
9. Decker, M., R. Zhao, C. M. Soukoulis, S. Linden, and M. Wegener, "Twisted split-ring-resonator photonic metamaterial with huge optical activity," *Opt. Lett.*, Vol. 35, 1593–1595, 2010.
10. Song, K., X. P. Zhao, Q. H. Fu, Y. H. Liu, and W. R. Zhu, "Wide-angle 90°-polarization rotator using chiral metamaterial with negative refractive index," *Journal of Electromagnetic Waves and Applications*, Vol. 26, Nos. 14–15, 1967–1976, 2012.
11. Kwon, D. H., P. L. Werner, and D. H. Werner, "Optical planar chiral metamaterial designs for strong circular dichroism and polarization rotation," *Opt. Express*, Vol. 16, 11802–11807, 2008.
12. Gansel, J. K., M. Thiel, M. S. Rill, M. Decker, K. Bade, V. Saile, G. Freymann, S. Linden, and M. Wegener, "Gold helix photonic metamaterial as broadband circular polarizer," *Science*, Vol. 325, 1513–1515, 2009.

13. Cheng, Y., Y. Nie, L. Wu, and R. Z. Gong, "Giant circular dichroism and negative refractive index of chiral metamaterial based on split-ring resonators," *Progress In Electromagnetics Research*, Vol. 138, 421–432, 2013.
14. Menzel, C., C. Helgert, C. Rockstuhl, E.-B. Kley, A. Taunermann, T. Pertsch, and F. Lederer, "Asymmetric transmission of linearly polarized light at optical metamaterials," *Phys. Rev. Lett.*, Vol. 104, 253902, 2010.
15. Wei, Z., Y. Cao, Y. Fan, X. Yu, and H. Li, "Broadband polarization transformation via enhanced asymmetric transmission through arrays of twisted complementary split-ring resonators," *Appl. Phys. Lett.*, Vol. 99, No. 22, 221907-3, 2011.
16. Huang, C., Y. Feng, J. Zhao, Z. Wang, and T. Jiang, "Asymmetric electromagnetic wave transmission of linear polarization via polarization conversion through chiral metamaterial structures," *Phys. Rev. B*, Vol. 85, No. 19, 195131, 2012.
17. Cheng, Y. Z., Y. Nie, X. Wang, and R. Z. Gong, "An ultrathin transparent metamaterial polarization transformer based on a twist-split-ring resonator," *Appl. Phys., A Mater. Sci. Process.*, Vol. 111, No. 1, 209–215, 2013.
18. Jackson, J. D., *Classical Electrodynamics*, 3rd Edition, Wiley, 1999.
19. Mutlu, M., A. E. Akosman, A. E. Serebryannikov, and E. Ozbay, "Asymmetric chiral metamaterial circular polarizer based on four U-shaped split ring resonators," *Opt. Lett.*, Vol. 36, No. 9, 1653–1655, 2011.
20. Ma, X., C. Huang, M. Pu, C. Hu, Q. Feng, and X. Luo, "Dual-band asymmetry chiral metamaterial based on planar spiral structure," *Appl. Phys. Lett.*, Vol. 101, 161901-4, 2012.
21. Ma, X., C. Huang, M. Pu, Y. Wang, Z. Zhao, C. Wang, and X. Luo, "Multi-band circular polarizer using planar spiral metamaterial structure," *Opt. Express*, Vol. 20, No. 14, 16050–16058, 2012.
22. Xie, L., H.-L. Yang, X. Huang, and Z. Li, "Multi-band circular polarizer using archimedean spiral structure chiral metamaterial with zero and negative refractive index," *Progress In Electromagnetics Research*, Vol. 141, 645–657, 2013.
23. Xu, H.-X., G.-M. Wang, M.-Q. Qi, T. Cai, and T. J. Cui "Compact dual-band circular polarizer using twisted Hilbert-shaped chiral metamaterial," *Opt. Express*, Vol. 21, No. 21, 24912–24921, 2013.
24. Yana, S. and G. A. E. Vandenbosch, "Compact circular polarizer based on chiral twisted double split-ring resonator," *Appl. Phys. Lett.*, Vol. 102, 103503, 2013.
25. Cheng, Y. Z., Y. Nie, C. Z. Cheng, X. Wang, and R. Z. Gong, "Asymmetric chiral metamaterial circular polarizer based on twisted split-ring resonator," *Applied Physics B*, doi:10.1007/s00340-013-5659-z, 2013, <http://link.springer.com/article/10.1007%2Fs00340-013-5659-z>.
26. Wu, L., Z. Y. Yang, Y. Z. Cheng, M. Zhao, R. Z. Gong, Y. Zheng, J. A. Duan, and X. H. Yuan, "Giant asymmetric transmission of circular polarization in layer-by-layer chiral metamaterials," *Appl. Phys. Lett.*, Vol. 103, 021903, 2013.
27. Zarifi, D., H. Oraizi, and M. Soleimani, "Improved performance of circularly polarized antenna using semi-planar chiral metamaterial covers," *Progress In Electromagnetics Research*, Vol. 123, 337–354, 2012.
28. Hong, Q., T. Wu, X. Zhu, R. Lu, and S. T. Wu, "Designs of wide-view and broadband circular polarizers," *Opt. Express*, Vol. 13, 8318–8331, 2005.
29. Ge, Z., M. Jiao, R. Lu, T. X. Wu, S. T. Wu, W. Y. Li, and C. K. Wei, "Wide-view and broadband circular polarizers for transmissive liquid crystal displays," *J. Display Technol.*, Vol. 4, 129–138, 2008.
30. Liu, N., H. Liu, S. Zhu, and H. Giessen, "Stereometamaterials," *Nat. Photon.*, Vol. 3, 157, 2009.
31. Liu, H., Y. M. Liu, T. Li, S. M. Wang, S. N. Zhu, and X. Zhang, "Coupled magnetic plasmons in metamaterials," *Phys. Status Solidi B*, Vol. 246, 1397, 2009.